

# Influence of post-liquefaction strain potential estimation on the accuracy of liquefaction severity number (LSN) hazard assessments

B.W. Maurer & R.A. Green

*Dept. of Civil & Environmental Eng., Virginia Tech, Blacksburg Virginia, United States.*

M. Cubrinovski & B.A. Bradley

*Dept. of Civil & Natural Resources Eng., University of Canterbury, Christchurch, New Zealand.*

**ABSTRACT:** The performance of any liquefaction hazard framework is intimately linked to the procedures used within it. For the Liquefaction Severity Number (LSN), post-liquefaction volumetric strain potential ( $\varepsilon_v$ ) is one of several inputs used to assess the damage-potential of liquefaction. However, as with other inputs to the LSN framework, different techniques exist for estimating  $\varepsilon_v$ , each of which could lead to different computed LSN values, and by corollary, different assessments of liquefaction hazard. Accordingly, this study investigates six techniques for estimating  $\varepsilon_v$  using analyses of 7,000 liquefaction case-studies from the 2010-2011 Canterbury earthquakes. Results indicate that: (1) the LSN hazard scale (i.e. relationship between computed LSN and expected liquefaction hazard) is dependent on the  $\varepsilon_v$  estimation method; (2) accounting for these different hazard scales, the  $\varepsilon_v$  estimation method had no effect on the accuracy of LSN hazard assessment, such that all performed equally well; however (3) a control model in which  $\varepsilon_v$  was removed performed best, suggesting that  $\varepsilon_v$  either provides no statistically distinguishable benefits in terms of prediction accuracy, or is presently accounted for in such a way that is not optimal.

## 1 INTRODUCTION

The 2010-2011 Canterbury, New Zealand, earthquake sequence (CES) induced pervasive and severe soil liquefaction in the Christchurch region, resulting in widespread damage to civil infrastructure. As illustrated by the CES and other recent earthquakes, accurate assessment of liquefaction hazard is critical. Towards this end, hazard frameworks have been proposed to link the factor of safety against liquefaction triggering at depth ( $FS_{liq}$ ) to the severity of liquefaction manifested at the ground surface, which serves as a pragmatic proxy for liquefaction damage potential. Within this realm, existing frameworks include: (1) the widely-used liquefaction potential index (LPI) (Iwasaki et al. 1978); (2) an Ishihara (1985) inspired variation of LPI, termed  $LPI_{ISH}$  (Maurer et al. 2015a); and (3) the liquefaction severity number (LSN) (van Ballegooy et al. 2014a), a variation of 1-D post-liquefaction settlement (e.g. Zhang et al. 2002). Central to all hazard frameworks are proposed decision thresholds corresponding to different levels of expected hazard. For example, Tonkin and Taylor (2013) proposed that little to no liquefaction manifestation is expected where  $LSN < 20$ ; moderate to severe liquefaction manifestation is expected where  $20 < LSN < 40$ ; and major manifestation of liquefaction is expected where  $LSN > 40$ .

Importantly, the efficacies of proposed threshold values are intimately linked to (Maurer et al., 2015b): (1) the approach used to select thresholds, and the assumed misprediction consequences implicit to such selections; (2) the assessed dataset; and (3) the adopted procedures used within the liquefaction hazard framework. The focus of this study is on the latter as it pertains to the performance of LSN, which is now widely used in New Zealand. LSN is defined as (van Ballegooy et al. 2014a):

$$LSN = 10 \int_0^{20} \varepsilon_v / z \, dz \quad (1)$$

where  $\varepsilon_v$  is the estimated post-liquefaction volumetric strain (%), and  $z$  is depth (m) below the ground surface. LSN thus assumes that the severity of liquefaction manifestation is a function of the cumulative thickness of liquefiable strata, the proximity of these strata to the ground surface, and the induced volumetric strain within these strata. Van Ballegooy et al. (2014a) proposed using the Zhang et al. (2002) approach to estimate  $\varepsilon_v$ , wherein values of equivalent-clean-sand-normalized CPT tip resistance ( $q_{c1Ncs}$ ) and computed  $FS_{liq}$  are used to assess a soil's post-liquefaction strain potential. The performance of LN

hazard assessment is therefore closely tied to the procedures used to determine  $FS_{liq}$  and  $\varepsilon_v$ . With respect to the former, several studies have investigated the influence of the procedure used to compute  $FS_{liq}$  on the accuracy of liquefaction hazard assessment. Among those commonly used in today's practice, the Idriss and Boulanger (2008) procedure has performed marginally better in analyzing data from the CES (Green et al. 2014; van Ballegooy et al. 2014a; Maurer et al. 2015c; 2015d) and is thus recommended by New Zealand Ministry of Business, Innovation, and Employment guidelines (MBIE, 2015).

Conversely, the influence of the procedure used to estimate  $\varepsilon_v$  is unknown. While significant differences exist among such procedures, the potential importance of these differences has never been thoroughly evaluated. Accordingly, this study investigates the influence of estimated  $\varepsilon_v$  on the accuracy of LSN hazard assessment using an analysis of 7,000 liquefaction case-studies from the CES, wherein six methods for estimating  $\varepsilon_v$  are used within the LSN framework. In the following, these six methods are first discussed in detail. The liquefaction case-studies to be analyzed, and additional methods used herein, are then summarized, followed by assessments of LSN performance.

### 1.1 Estimating Post-Liquefaction Volumetric-Strain ( $\varepsilon_v$ )

While attempts to estimate  $\varepsilon_v$  trace to earlier studies (e.g. Lee and Albaisa 1974), current CPT-based methods for estimating  $\varepsilon_v$  are often rooted in the work of Nagase and Ishihara (1988), who conducted cyclic simple shear tests on saturated sands of varying relative density ( $D_r$ ). Based largely on the results of Nagase and Ishihara (1988), Ishihara and Yoshimine (1992) proposed a series of curves, shown in Figure 1a, for estimating  $\varepsilon_v$  as a function of  $FS_{liq}$  and  $D_r$ . Using a correlation proposed by Tatsuoka et al. (1990) to convert from  $D_r$  to  $q_{c1N}$ , Zhang et al. (2002) converted the Ishihara and Yoshimine (1992) curves into a form suitable for use with CPT-based procedures for computing  $FS_{liq}$ , as shown in Figure 1b. However, to better capture trends identified by Ishihara and Yoshimine (1992), additional curves are developed in this study (Fig. 1b) for  $FS_{liq} = 0.95, FS_{liq} = 0.96 \dots FS_{liq} = 0.99$  to supplement those of Zhang et al. (2002). As evident in Figure 1b, these curves are needed to accurately represent the behaviour identified by Ishihara and Yoshimine (1992), whereas linear interpolations between the  $FS_{liq} = 0.9$  and  $FS_{liq} = 1$  curves often fail to do so. It is also noteworthy that the Zhang et al. (2002) curves were developed using a correlation to  $q_{c1N}$  (i.e. normalized tip resistance, *uncorrected* for fines), but are proposed for use with values of  $q_{c1Ncs}$ . This simplification, justifications for which are given by Zhang et al. (2002) and Idriss and Boulanger (2008), is used throughout this study.

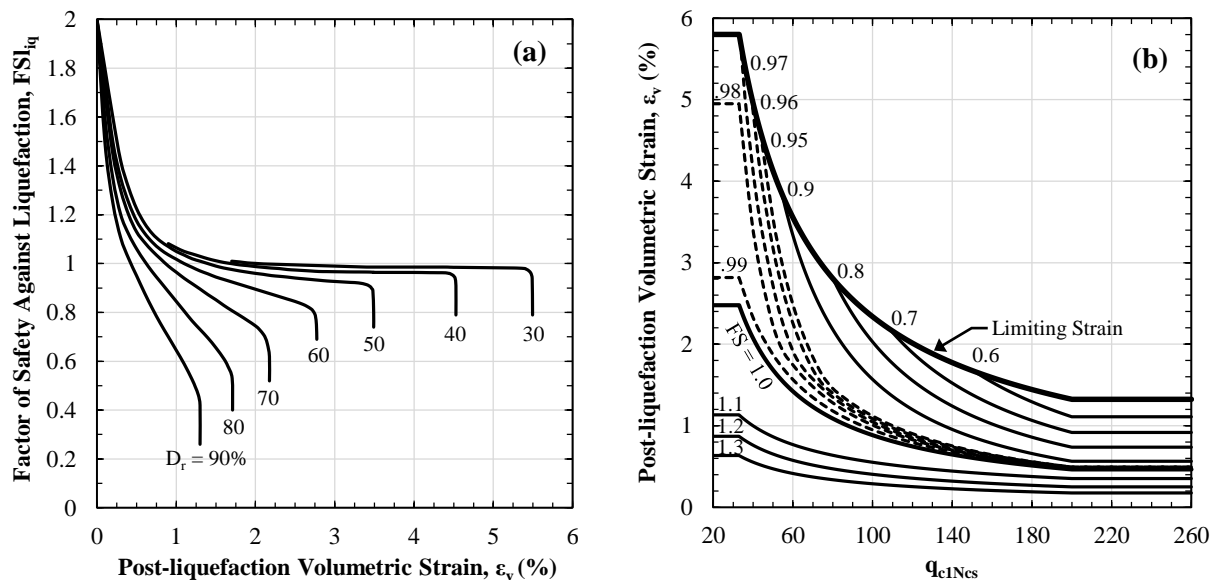


Figure 1. (a) Curves for estimating post-liquefaction volumetric-strain ( $\varepsilon_v$ ) as a function of the factor of safety against liquefaction ( $FS_{liq}$ ) and initial relative density ( $D_r$ ) (after Ishihara and Yoshimine 1992); (b) curves derived from (a) for estimating  $\varepsilon_v$  as a function of  $FS_{liq}$  and equivalent clean sand normalized CPT tip resistance ( $q_{c1Ncs}$ ), as proposed by Zhang et al. (2002) utilizing Equation (2), with curves added for this study (after Zhang et al. 2002).

Problematically, while the Zhang et al. (2002) method for estimating  $\varepsilon_v$  is widely used in practice, it is rigidly tied to the Tatsuoka et al. (1990) correlation developed for Toyoura (Japan) sand, defined as:

$$D_r (\%) = -85 + 76 \log(q_{c1N}) \quad (2)$$

where  $D_r$  and  $q_{c1N}$  are as previously defined. Thus, if Equation (2) performs poorly for soils elsewhere, the resulting  $\varepsilon_v$  estimates could be inaccurate. Alternative correlations include that of Idriss and Boulanger (2003), adapted from Salgado et al. (1997), and defined as:

$$D_r = 0.465 \left( \frac{q_{c1N}}{C} \right)^{0.264} - 1.063 \quad (3)$$

where  $C$  is a soil-specific constant. Idriss and Boulanger (2003) used  $C = 0.9$  in analyzing global liquefaction case studies, whereas  $C$  ranged from 0.64 to 1.55 for soils studied by Salgado et al. (1997). Plotted in Figure 2 are Equations (2) and (3), wherein 3 values of  $C$  are adopted for the latter ( $C = 0.64, 0.9, 1.55$ ). It can be seen that large differences exist among the selected correlations, which could lead to different estimates of  $\varepsilon_v$ , and thus, different LSN hazard assessments.

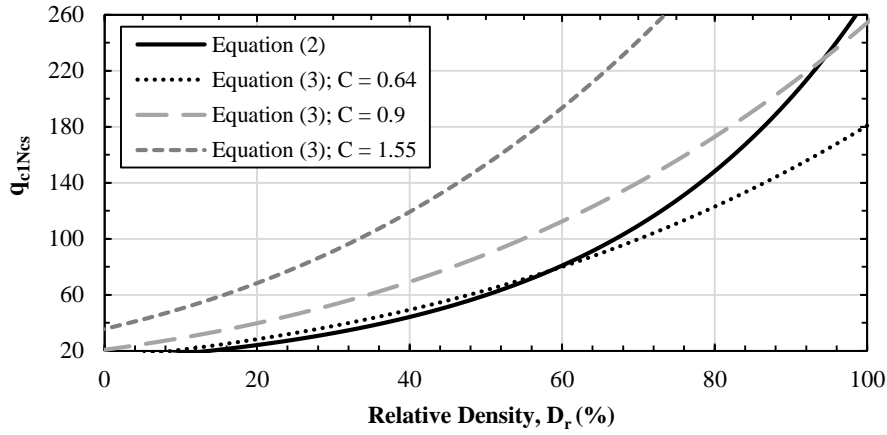


Figure 2. Correlations relating equivalent clean sand normalized CPT tip resistance ( $q_{c1Ns}$ ) to relative density ( $D_r$ ).

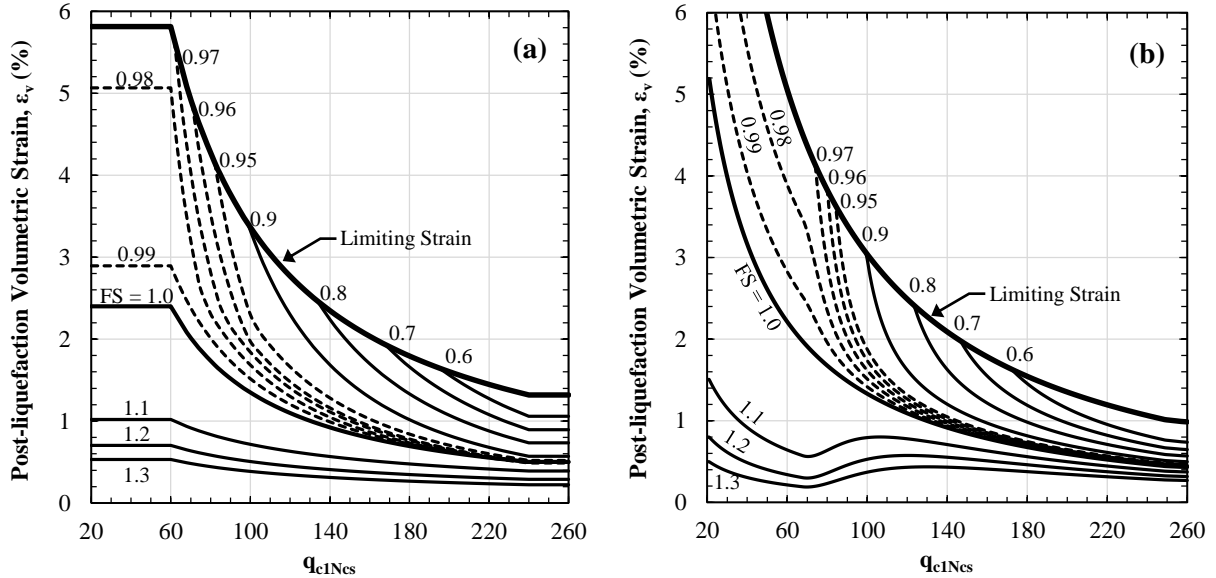


Figure 3. Curves derived from Figure 1a for estimating post-liquefaction volumetric-strain ( $\varepsilon_v$ ) as a function of the factor of safety against liquefaction ( $FS_{liq}$ ) and equivalent clean sand normalized CPT tip resistance ( $q_{c1Ns}$ ), herein developed utilizing Equation (3) with  $C = 0.9$ : (a) in the style of Zhang et al. (2002); and (b) using approximate, continuous solutions proposed by Yoshimine et al. (2006).

Accordingly, utilizing variants of Equation (3), four alternatives to the Zhang et al. (2002) method are derived from Ishihara and Yoshimine (1992). *First*, as shown in Figure 3a, curves are developed a la Zhang et al. (2002) utilizing Equation (3) with  $C = 0.9$ , as adopted by Idriss and Boulanger (2003). These curves generally result in higher  $\varepsilon_v$  estimates relative to Zhang et al. (2002). *Second*, as shown in Figure 3b, curves are developed using the continuous function proposed by Yoshimine et al. (2006) which

approximates the Ishihara and Yoshimine (1992) relations, wherein Equation (3) is again used with  $C = 0.9$ . Notably, the Zhang et al. (2002) approach suffers from two limitations solved by the Yoshimine et al. (2006) function: (1) it is laborious, such that developing curves for multiple  $D_r - q_{c1N}$  correlations is impractical; and (2) the resulting curves are defined by discrete functions, such that interpolation is required to estimate  $\varepsilon_v$ . It can be seen in Figure 3a and 3b that  $\varepsilon_v$  estimates are very similar using these two approaches, but that  $\varepsilon_v$  is not bound to the Ishihara and Yoshimine (1992) parameter space (i.e.  $30\% < D_r < 90\%$ ) in the latter. The Yoshimine et al. (2006) function is thus recommended for its pragmatic benefits. *Third* and *fourth*,  $\varepsilon_v$  is estimated using the Yoshimine et al. (2006) function and Equation (3) with respective  $C$  values of 0.64 and 1.55, the significance of which are as mentioned previously.

In addition, a “control” method is developed. To assess the possibility that manifestation severity is not influenced explicitly by  $D_r$  (i.e. beyond its influence in procedures that compute  $FS_{liq}$ ),  $\varepsilon_v$  is set to an arbitrary value of 1% for all  $FS_{liq} < 1$ , and 0 otherwise. The six aforementioned methods for estimating  $\varepsilon_v$  are summarized in Table 1 and henceforth referred to as S1, S2, S3, S4, S5, and C1, respectively (Table 1, column 1).

**Table 1. Summary of  $\varepsilon_v$  estimation methods to be assessed in the LSN framework.**

ID	Derived from Ishihara & Yoshimine 1992	$D_r - q_{c1N}$ Correlation Utilized	Function(s)
S1	✓	Eq. (2)	Zhang et al. 2002
S2	✓	Eq. (3); $C = 0.9$	Available on request (a la Zhang et al. 2002)
S3	✓	Eq. (3); $C = 0.9$	Yoshimine et al. 2006
S4	✓	Eq. (3); $C = 0.64$	Yoshimine et al. 2006
S5	✓	Eq. (3); $C = 1.55$	Yoshimine et al. 2006
C1	✗	N/A	$\varepsilon_v (\%) = \begin{cases} 1 & \text{for } FS_{liq} < 1 \\ 0 & \text{for } FS_{liq} \geq 1 \end{cases}$

### 3 DATA AND METHODOLOGY

#### 3.1 CPT Soundings

This study utilizes 3,500 CPT soundings performed at sites where the severity of liquefaction manifestation was well-documented following both the Darfield and Christchurch earthquakes, resulting in 7,000 liquefaction case studies. Soundings were performed on various dates following the start of the CES, to include dates prior to, and following, the Christchurch earthquake. The CPT data is assumed to be unaffected by the date of the sounding (i.e., by the quantity and relative timing of prior earthquakes), as supported by Lees et al. (2015). In compiling the 7,000 case studies, CPT soundings were first rejected if: (1) performed at sites where the predominant manifestation of liquefaction was lateral spreading; (2) the depth of “pre-drill” significantly exceeded the estimated depth to ground water, or (3) believed to have prematurely terminated on shallow gravels, as inferred from an Anselin (1995) Local Morans  $I$  analysis. For further discussion of CPTs and this geostatistical analysis, see Maurer et al. (2014).

#### 3.2 Liquefaction Severity

Observations of liquefaction and the severity of manifestation were made by the authors for each CPT sounding location following both the Darfield and Christchurch earthquakes. CPT sites were assigned one of six damage classifications, as described in Green et al. (2014). Of the 7,000 cases compiled, 49% are cases of “no manifestation,” and 51% are cases where manifestations were observed and classified.

#### 3.3 Estimation of Peak Ground Acceleration (PGA)

To evaluate  $FS_{liq}$  for use in computing LSN values, PGAs at the ground surface were computed using

the Bradley (2013a) model, which combines unconditional PGA distributions estimated by the Bradley (2013b) ground motion prediction equation, recorded PGAs from strong motion stations, and the spatial correlation of intra-event residuals to compute conditional PGA distributions at sites of interest.

### 3.4 Estimation of Ground Water Table (GWT) Depth

Given the sensitivity of liquefaction hazard to GWT depth (e.g. Maurer et al. 2014), accurate estimates of the GWT are critical. For this study, GWT depths were sourced from the event-specific regional ground water models of van Ballegooy et al. (2014b). These models, which reflect seasonal and localized fluctuations across the region, were derived in part using monitoring data from ~1000 piezometers and provide a best-estimate of GWT depths immediately prior to the Darfield and Christchurch earthquakes.

### 3.5 Liquefaction Evaluation and LSN

$FS_{liq}$  was computed using the deterministic procedure proposed by Idriss and Boulanger (2008), where the soil behavior type index,  $I_c$ , was used to identify non-liquefiable strata; soils with  $I_c > 2.4$  were assumed non-liquefiable, per Maurer et al. (2015d). For I&B08, fines content (FC) is required to compute normalized tip resistances; as such, FC values were estimated using the  $I_c$ -FC correlation proposed by Boulanger and Idriss (2014). LSN was computed for each of the 7,000 case studies per Equation (1), wherein  $\varepsilon_v$  was estimated using each of the six methods summarized in Table 1.

### 3.6 Receiver Operating Characteristic (ROC) Analyses

To investigate the significance of the  $\varepsilon_v$  estimation method used in the LSN framework, a standard analysis is needed to assess the performance of LSN hazard assessment. More specifically, for the six LSN variants, this analysis must: (1) evaluate their relative efficacies, independent of LSN decision thresholds; and (2) identify for each the optimum threshold value at which performance is optimized. Receiver operating characteristic (ROC) analyses are herein adopted for this purpose.

In using LSN to predict liquefaction manifestation, the distributions of “positives” (i.e. liquefaction manifestation is observed) and “negatives” (i.e. no liquefaction manifestation is observed) overlap when the frequencies of the distributions are expressed in terms of computed LSN values. Optimal LSN decision thresholds are selected considering the rates of true positives ( $R_{TP}$ ) (i.e. liquefaction is observed, as predicted) and false positives ( $R_{FP}$ ) (i.e. liquefaction is predicted, but is not observed). Setting the threshold too low will result in a higher  $R_{FP}$ , the cost of which could be excessive spending on engineering design and construction (e.g. ground improvement costs). Conversely, setting the threshold too high results in a higher rate of false negatives (i.e. liquefaction is observed when it is predicted not to occur), the cost of which is liquefaction-induced damage (e.g. lost productivity, property damage, and reconstruction costs, among others). Thresholds should thus be selected so as to minimize these costs.

ROC curves plot  $R_{TP}$  versus  $R_{FP}$  for varying threshold values. Figures 4a and 4b illustrate the relationship among the positive and negative distributions, the threshold value, and the ROC curve. Figure 4b also illustrates how a ROC curve is used to assess the efficiency of a diagnostic test and select an optimum threshold. In ROC space, random guessing is indicated by a 1:1 line through the origin (i.e. equivalent correct and incorrect predictions), while a perfect model plots as a point at (0,1), indicating the existence of a threshold value which perfectly segregates the dataset (i.e. all cases with manifestation have LSN above the threshold; all cases without manifestation have LSN below the threshold). While no single parameter can fully characterize model performance, the area under a ROC curve (AUC) is commonly used for this purpose, where AUC is statistically equivalent to the probability that sites with manifestation have higher computed LSN than sites without manifestation (e.g. Fawcett 2005). As such, increasing AUC indicates better model performance. The optimum decision threshold, or optimum operating point (OOP), is defined herein as the threshold LSN value which minimizes the rate of misprediction [i.e.  $R_{FP} + (1 - R_{TP})$ ]. As such, contours of the quantity  $[R_{FP} + (1 - R_{TP})]$  represent points of equivalent performance in ROC space, as shown in Figure 4b. For further overview of ROC analyses, and for demonstration of how project-specific misprediction consequences can be incorporated into ROC analyses, the reader is referred to Fawcett (2005) and Maurer et al. (2015b), respectively.

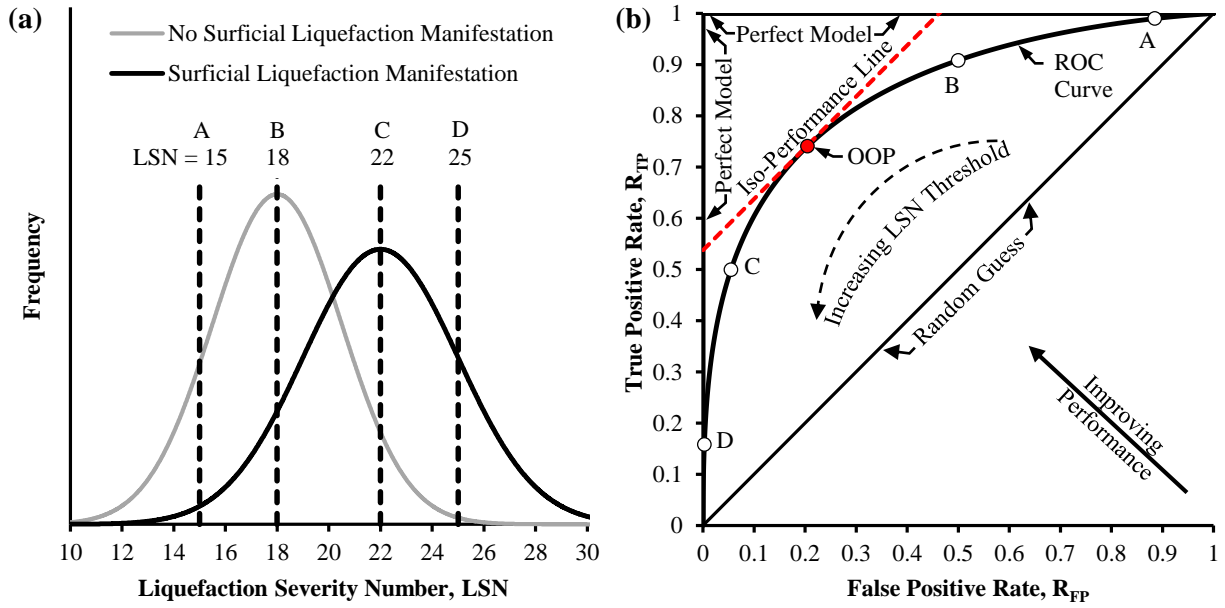


Figure 4. ROC analyses: (a) frequency distributions of liquefaction manifestation and no liquefaction manifestation as a function of LSN; (b) corresponding ROC curve, and illustration of how a ROC curve is used to assess the efficiency of a diagnostic test. The optimum operating point (OOP) indicates the LSN decision threshold for which the rate of misprediction is minimized.

#### 4 RESULTS AND DISCUSSION

In Figure 5a, ROC curves are plotted to evaluate the accuracy of LSN hazard assessment for 7,000 liquefaction case studies from the CES, wherein six variants for estimating  $\varepsilon_v$  are assessed. More specifically, the performance evaluated in Figure 5 is that of LSN to predict liquefaction manifestations likely to damage infrastructure. In the adopted classification scheme (Green et al. 2014), “marginal” manifestations are characterized by a trace amount of water or ejecta and are likely to be non-damaging, whereas “moderate” to “severe” manifestations are likely to coincide with damage. Shown in Figure 5b is a magnified view of the optimal-performance area in ROC space, wherein the optimal LSN decision threshold is identified for models S1 through S5.

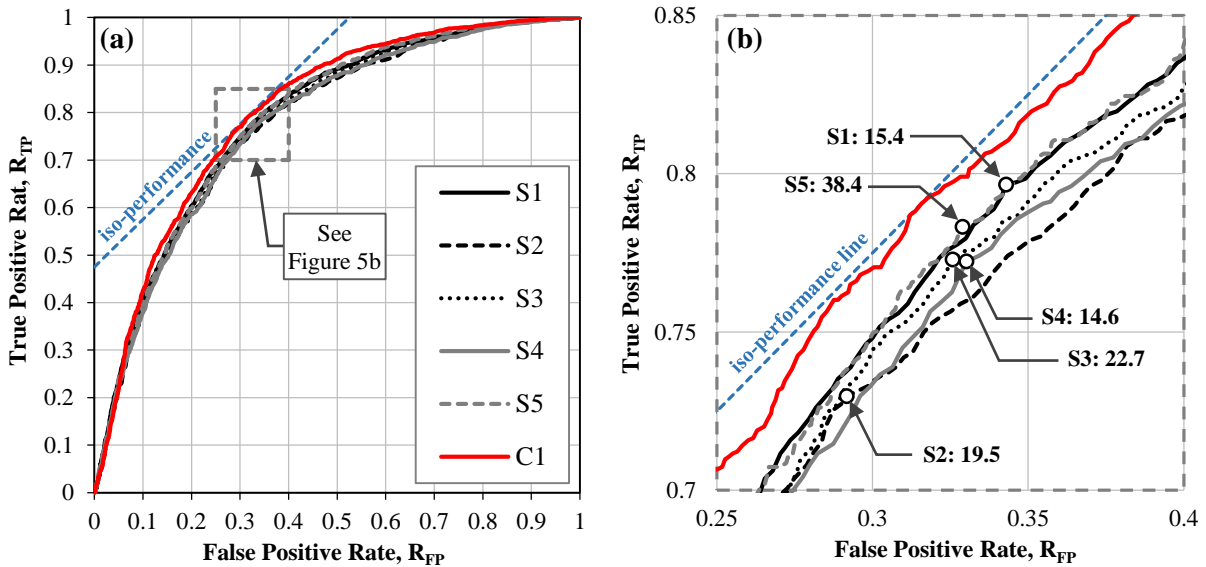


Figure 5. (color) (a) ROC analyses of six LSN variants in predicting liquefaction likely to cause damage; (b) magnified view of optimal-performance area, wherein optimal LSN thresholds are identified for S1 through S5.

It can be seen in Figure 5a that models S1 through S5 have nearly identical performance, such that none of the five methods for estimating  $\varepsilon_v$  result in more (or less) accurate LSN hazard assessments for the considered case studies. In this regard, the measured AUCs range from 0.78 (S2, S3, S4) to 0.79 (S1 and S5). To place this performance in context, AUCs of 0.5 and 1.0 respectively indicate random guessing and a perfect model. However, it can be seen in Figure 5b that the LSN threshold at which performance is optimal varies significantly, ranging from LSN = 14.6 for S4, to LSN = 38.4 for S5. Thus, if optimal thresholds obtained from an analysis using one  $\varepsilon_v$  estimation method are applied to forward analyses wherein a different method is used, the resulting hazard assessments could be erroneous. Notably, the optimal thresholds for models S1 through S4 are reasonably consistent with that proposed by Tonkin and Taylor (2013) for predicting “moderate to severe” liquefaction manifestations (i.e. LSN = 20).

Interestingly, it can be seen in Figures 5a and 5b that “control” model C1 performs best, with measured AUC of 0.80. The leading performance of C1 indicates that the utility of  $\varepsilon_v$  is unclear. More specifically, this result suggests that: (1)  $\varepsilon_v$  is not a statistically significant variable for predicting liquefaction manifestation (i.e. beyond its inherent accounting for by procedures that compute  $FS_{liq}$ , see Dobry 1989); and/or (2)  $\varepsilon_v$  is accounted for in the LSN framework in such a way that is not optimal; and/or (3) the methods adopted for estimating  $\varepsilon_v$  (i.e. S1 through S5) do not accurately portray the behavior of soils in the case studies assessed herein. With respect to the latter, additional methods for estimating  $\varepsilon_v$  in the LSN framework could be assessed in future studies.

Importantly, even the best-performing model has potential for significant improvement. Operating at its optimum threshold, C1 has overall accuracy of 71%, indicating that 29% of liquefaction case studies are predicted incorrectly. While liquefaction triggering has garnered significant research and debate, the mechanics of liquefaction manifestation have received less attention, and seemingly, are less well understood. In this regard, further research is needed to fully elucidate and quantify influential factors.

## 5 CONCLUSIONS

Utilizing 7,000 liquefaction case-studies from the CES, this study investigated the influence of the method used to estimate  $\varepsilon_v$  within the LSN framework on the accuracy of resultant hazard assessments. The results are as follows: (1) the LSN hazard scale (i.e. relationship between computed LSN and expected liquefaction hazard) is dependent on the  $\varepsilon_v$  estimation method, and as such, LSN thresholds obtained from analyses using one method should not be applied to forward analyses wherein a different method is used; (2) accounting for these different hazard scales, the selected  $\varepsilon_v$  estimation method had no effect on the accuracy of LSN hazard assessment, such that all methods performed equally well; however, (3) a control model in which  $\varepsilon_v$  was removed from the LSN framework performed best, suggesting that  $\varepsilon_v$  either provides no statistically distinguishable benefits in terms of prediction accuracy, or is presently accounted for in such a way that is not optimal. Of course, the findings presented are based on a dataset from the CES, and their applicability to other datasets, or to methodologies different from that used herein, is unknown.

## 6 ACKNOWLEDGEMENTS

This study is based on work supported by the US National Science Foundation (NSF) grants CMMI 1030564, CMMI 1407428, and CMMI 1435494, and US Army Engineer research and Development Center (ERDC) grant W912HZ-13-C-0035. The authors also acknowledge the Canterbury Geotechnical Database and its sponsor EQC for providing data used in this study. However, any opinions, findings, and conclusions or recommendations expressed in this paper are those of the authors and do not necessarily reflect the views of NSF, ERDC, or EQC.

## REFERENCES:

- Anselin L. 1995. Local Indicators of Spatial Association—LISA, *Geographical Analysis*; 27(2): 93–115.
- Boulanger RW & Idriss IM. 2014. CPT and SPT based liquefaction triggering procedures, *Report No. UCD/CGM-14/01*, Center for Geotech. Modelling, Dept. of Civil and Environ. Eng., UC Davis, CA, USA.
- Bradley BA. 2013a. Site-specific and spatially-distributed ground motion intensity estimation in the 2010-2011 Christchurch earthquakes, *SDEE*, 48: 35-47.

- Bradley BA. 2013b. A New Zealand-specific pseudo-spectral acceleration ground-motion prediction equation for active shallow crustal earthquakes based on foreign models, *BSSA*, 103(3): 1801-1822.
- Dobry R. 1989. Some basic aspects of soil liquefaction during earthquakes, *Earthquake Hazards and The Design of Constructed Facilities in the Eastern United States* (KH Jacob and CJ Turkstra, eds.), Annals of the New York Academy of Sciences, 558: 172-182.
- Fawcett T. 2005. An introduction to ROC analysis, *J of Pattern Recognition Letters*, 27(8): 861-874.
- Green RA, Cubrinovski, M, Cox, B, Wood, C, Wotherspoon, L, Bradley, B, Maurer, B. 2014. Select Liquefaction Case Histories from the 2010-2011 Canterbury Earthquake Sequence, *Earthquake Spectra*, 30(1): 131-153.
- Idriss IM & Boulanger RW. 2008. Soil liquefaction during earthquakes, *Monograph MNO-12*, Earthquake Engineering Research Institute, Oakland, CA, 261 pp.
- Idriss IM & Boulanger RW. 2003. Relating  $K_q$  and  $K_\sigma$  to SPT blow count and to CPT tip resistance for use in evaluating liquefaction potential, *2003 Dam Safety Conference*, Minneapolis, MN, USA.
- Ishihara K. 1985. Stability of natural deposits during earthquakes, *11<sup>th</sup> International Conference on Soil Mechanics and Foundation Engineering*, San Francisco, CA, USA, 1: 321-376.
- Iwasaki T, Tatsuoka F, Tokida K, Yasuda S. 1978. A practical method for assessing soil liquefaction potential based on case studies at various sites in Japan, *2nd Int. Conf. on Microzonation*, San Francisco, USA, 1978.
- Lee KL and Albaisa A. 1974. Earthquake induced settlements in saturated sands, *J Soil Mechanics and Foundations*, 100(4): 387-406.
- Lees JJ, Ballagh RH, Orense RP, van Ballegooy S. 2015. CPT-based analysis of liquefaction and re-liquefaction following the Canterbury earthquake Sequence, *SDEE*, *In Press*.
- Maurer BW, Green RA, Cubrinovski M, Bradley B. 2014. Evaluation of the liquefaction potential index for assessing liquefaction hazard in Christchurch, New Zealand. *J Geotech Geoenviron Eng.*, 140(7), 04014032.
- Maurer BW, Green RA, Cubrinovski M, Bradley B. 2015a. Moving towards an improved index for assessing liquefaction hazard: lessons from historical data, *Soils and Foundations*, 55(4): 778-787.
- Maurer BW, Green RA, Cubrinovski M, Bradley B. 2015b. Calibrating the liquefaction severity number (LSN) for varying misprediction economies: a case study in Christchurch, New Zealand, *6th Int. Conf. on Geotechnical Earthquake Engineering*, Christchurch, New Zealand, *In Press*.
- Maurer BW, Green RA, Cubrinovski M, Bradley B. 2015c. Assessment of CPT-based methods for liquefaction evaluation in a liquefaction potential index (LPI) framework, *Geotechnique*, 65(5): 328-336.
- Maurer BW, Green RA, Cubrinovski M, Bradley B. 2015d. Fines-content effects on liquefaction hazard evaluation for infrastructure during the 2010-2011 Canterbury, New Zealand earthquake sequence, *SDEE* 76: 58-68.
- MBIE. 2015. Repairing and rebuilding houses affected by the Canterbury earthquakes, Ver. 3a, Ministry of Business, Innovation, and Employment, Wellington, New Zealand.
- Nagase H, Ishihara K. 1988. Liquefaction-induced compaction and settlement of sand during earthquakes, *Soils and Foundations*, 28(1):66-76.
- Salgado R, Mitchell JK, Jamiolkowski, M. 1997. Cavity expansion and penetration resistance in sands, *J Geotech Geoenviron Eng.* 123(4): 344-354.
- Tatsuoka F, Zhou S, Sato T, Shibuya S. 1990. Evaluation method of liquefaction potential and its application. Report on seismic hazards on the ground in urban areas. Ministry of Education of Japan, Tokyo, Japan.
- Tonkin & Taylor (2013). Liquefaction vulnerability study, *T&T Ref: 52020.0200/v.1.0*, Christchurch, NZ.
- van Ballegooy, S, Malan, P, Lacrosse, V, Jacka, ME, Cubrinovski, M, Bray, JD, O'Rourke, TD, Crawford, SA, and Cowan, H. 2014a. Assessment of liquefaction-induced land damage for residential Christchurch, *Earthquake Spectra*, 30(1): 31-55.
- van Ballegooy S, Cox SC, Thurlow C, Rutter HK, Reynolds T, Harrington G, Fraser J, and Smith T. 2014b. Median water table elevation in Christchurch and surrounding area after the 4 September 2010 Darfield earthquake: Version 2, *GNS Science Report 2014/18*, 2014b.
- Yoshimine M, Nishizaki H, Amano K, Hosono Y. 2006. Flow deformation of liquefied sands under constant shear load and its application to analysis of flow slide in infinite slope. *SDEE*, 26: 253-264.
- Zhang G, Robertson PK, Brachman R. 2002. Estimating Liquefaction Induced Ground Settlements from CPT, *Canadian Geotechnical Journal*, 39: 1168-1180.